Microchimica Acta (2024) 191:593
https://doi.org/10.1007/s00604-024-06655-z

RESEARCH

Platinum-perovskite nanocomposite-based Exosensor for specific detection of prostate cancer in clinical settings

Ehsan Dezhakam[1] · Elham Mahmoudi[2] · Abdolhossein Naseri[1] · Reza Rahbarghazi[3,4] · Ibrahim Isildak[5] · Balal Khalilzadeh[3] · Aligholi Niaei[2,6] · Nagihan Delibas[6] · Ali Coruh[6]

Received: 29 May 2024 / Accepted: 27 August 2024

Abstract

Exosomes, extracellular vesicles (EVs) with an average size of 50–150 nm, transfer various biomolecules and exchange signaling molecules between cells in a paracrine manner. Molecular investigations have revealed that EVs can reflect real-time metabolic changes in normal- and cancer-origin cells and thus harbor valid diagnostic biomarkers. Despite these advantages, the detection of low concentrations of cancer cell EVs in biological fluids is still a great challenge. Here, a new electrochemical Exosensor based on platinum-perovskite is developed for the direct detection of EVs using a biotinylated monoclonal CD63 antibody as a capture element. The label-free method exhibited higher sensitivity with a lower limit of quantification of 2000 EVs/μL with a dynamic linear range (LDR) of 2000 to 14,000 EVs/μL compared with other available methods. To enhance the selectivity of detection, EVs were simultaneously sandwiched between secondary antibodies of PSA (prostate-specific antigen), as an FDA-approved prostate cancer biomarker. Data indicated that this Exosensor can distinguish normal and cancer EVs in samples from healthy individuals and prostate cancer patients. Taken together, this technology offers a unique approach to label-free quantification of EVs and cancer detection in the early stages.

Keywords Prostate-specific antigen · Extracellular vesicles · Exosomes · Electrochemical Exosensor · Modified glassy carbon electrode · Differential pulse voltammetry · Perovskite

Introduction

Exosomes (Exos) are double phospholipid membrane extracellular vesicles (EVs) with an average size of 50 to 150 nm [1, 2]. Compared to other EV types such as apoptotic bodies and microvesicles, Exos are produced by the activity of the endosomal system using different molecular types of machinery such as ESCRT, tetraspanins, and SNARE factors [3]. Several investigations have revealed that EVs are rich in protein, miRNA, and DNA and play an essential role in cell-to-cell communication. These nanosized particles can reflect real-time changes in the metabolic status of parent origin cells, indicating EVs as a valid diagnostic tool [1, 4]. Besides their diagnostic roles, EVs can be involved in the promotion of cancer cell proliferation, angiogenesis, and metastasis [5–7]. EVs released by cancer cells can easily distribute in several biofluids such as blood and thus could be used for monitoring and diagnosis the several pathologies especially anaplastic changes [8]. According to published data, identifying prostate cancer antigens in the early stages

✉ Abdolhossein Naseri
ab.naseri@gmail.com

✉ Balal Khalilzadeh
balalkhalilzadeh@gmail.com; khalilzadehb@tbzmed.ac.ir

[1] Department of Analytical Chemistry, Faculty of Chemistry, University of Tabriz, Tabriz, Iran

[2] Catalyst and Reactor Research Lab, Department of Chemical & Petroleum Engineering, University of Tabriz, Tabriz, Iran

[3] Stem Cell Research Center (SCRC), Tabriz University of Medical Sciences, Tabriz, Iran

[4] Department of Applied Cell Sciences, Faculty of Advanced Medical Sciences, Tabriz University of Medical Sciences, Tabriz, Iran

[5] Department of Bioengineering, Faculty of Chemistry-Metallurgy, Yildiz Technical University, 34220 Istanbul, Turkey

[6] Department of Physics, Faculty of Science, University of Sakarya, Sakarya, Turkey

Published online: 12 September 2024

of development can increase the probability of a treatment intervention and increase survival rates from 10 to 90% [9].

Recently, some methods such as nanoparticle tracking analysis (NTA) [10], flow cytometry [11], western blotting [12], and ELISA [13] have been used for the detection of EVs or related proteins. NTA can be used when the concentration of EVs is between 10^7 and 10^9 particles mL^{-1}, but when the concentration is lower than that, quantification is laborious. NTA is mainly used for particle size and potential distribution detection. Flow cytometry can be applied for high-throughput detection, but light scattering from EVs with particle sizes < 100 nm is weak and cannot be accurately quantified. ELISA and western blot analyses require a large sample volume and the sensitivity of both of them is limited.

Since EV particles are limited in peripheral blood in the early stages of cancers, early and precise detection is difficult due to the low sensitivity of traditional detection methods [14]. Therefore, there is an urgent need for accurate diagnostic approaches with high sensitivity and selectivity for the early detection of EVs [15]. Recently, biosensors, including recognition elements and energy transducers, have received great interest in the detection of biomolecules, especially EVs [16]. After the detection of target molecules, biosensors can generate signals that can be read by alternative signal transduction elements. Signal transduction elements mainly include colorimetry [17], surface plasmon resonance (SPR) [18], surface-enhanced Raman scattering (SERS) [19], fluorescence [20], electrochemiluminescence (ECL) [21], field-effect transistors (FETs) [14, 22] as gate-controlled structures with visible light [23], and electrochemistry [24, 25]. The electrochemical biosensor enables the conversion of identification information of biological molecules into electrochemical signals of current, potential, and impedance [26]. Furthermore, electrochemical biosensors have been recognized as a vital tool due to their inherent advantages such as rapid analysis, cost/time effective, easy operation, portability, miniaturization, selectivity, and high sensitivity [27–29].

Nanomaterials have specific features like reactive surface topography, better mechanical features, quantum effects, superior sensitivity, high surface area, and catalytic activities [30, 31]. These properties make them a more desirable recourse for biosensing approaches compared to the other available materials [32]. Over the past few decades, perovskite oxides, characterized by their cubic-symmetry structure represented by the chemical formula ABO_3 (where A: rare-earth or alkaline earth cations, B: a transition cation), have gained considerable significance as a crucial group of catalysts [33–35]. A key feature of perovskites is their capacity for partial or/and total substitution of different cations at the A and B sites, resulting in a versatile and adaptable structure (denoted as $A_{1-x}A'_xB_{1-y}B'_yO_3$), which exhibits tunable physical–chemical properties [36–39]. These unique characteristics have led to a significant focus on perovskite oxides in various applications, including their utilization as catalysts and electrocatalysts in processes such as De-NO_x and dry reforming [40], supercapacitors [41], biosensors [42], water splitting [43–45], fuel cells [46], and batteries [47].

However, one notable drawback of perovskite oxides is their inherent low electron conductivity, primarily attributed to the high calcination temperatures employed during their synthesis [48]. On the other hand, noble metals such as palladium and platinum have garnered significant interest due to their exceptional conductivity, facilitating efficient electron transport [49]. To overcome this limitation, partial substitution of noble metals in small concentrations at the B site of perovskites has known a promising solution.

Herein, we established a label-free electrochemical Exosensor using Pt-perovskite for the quantification of EVs derived from prostate cancer cells. Also, this proposed method efficiently discriminated between normal and cancer EV prostate cancer patient sera compared to control samples. Overall, the developed Exosensor shows a potential value for the detection of EVs in the screening and early diagnosis of cancers.

Experimental section

Chemicals and materials

$La(NO_3)_3{\cdot}6H_2O$, $Fe(NO_3)_3{\cdot}9H_2O$, $Mn(NO_3)_2{\cdot}4H_2O$, $Pt(NH_3)_4{\cdot}2H_2O$, glycine, $NH_3{\cdot}H_2O$, and 6-mercaptohexanol (MCH) were purchased from Sigma-Aldrich. Biotinylated human monoclonal CD63 antibody (Clone: H5C6, Cat: 353,018) and purified streptavidin protein were purchased from BioLegend Company. Anti-PSA was purchased from Abcam (ab76113). H_2SO_4, KH_2PO_4, Na_2HPO_4, KCl, $K_4[Fe(CN)_6]$, and $K_3[Fe(CN)_6]$ were obtained from Merck company.

Apparatus

All electrochemical measurements were carried out with a conventional three-electrode system on RadStat-10 potentiostat/galvanostat electrochemical analyzer (Kianshardanesh, Iran) including a reference electrode (Ag/AgCl), a counter electrode (platinum wire), and a working electrode (glassy carbon with 2-mm diameter). An ultrasonic device (Strasonic 35) and a magnetic stirrer (Heidolph) were applied for the homogenization of the prepared solutions. A centrifuge (Beckman) was used to separate EVs from the serum samples.

Composite characterization

The scanning electron microscopy (SEM) images and semi-quantitative amounts of the elements were acquired by a Quanta FEG 450 instrument. Transmission electron microscopy (TEM) was carried out on the Hitachi HighTech HT7700 to complete the structural analysis. The X-ray diffraction (XRD) pattern was obtained using a Tongda TD-3700 X-ray diffractometer from China. Cu-Kα radiation with a wavelength (λ) of 1.5406 Å was used, and the scanning range spanned from 10 to 90°. Also, X-ray photoelectron spectroscopy (XPS) measurements were carried out using a Thermo Scientific K-Alpha instrument, with Al Kα emission as the excitation source for elemental analysis and characterization.

Synthesis of $La(Fe_{0.7}Mn_{0.3})_{0.98}Pt_{0.02}O_3$

To synthesize $La(Fe_{0.7}Mn_{0.3})_{0.98}Pt_{0.02}O_3$ perovskite oxide, the combustion sol–gel method was employed, as outlined in reference [50]. First, the calculated amounts of nitrates were dissolved in deionized water and heated to 80 °C. Subsequently, glycine was added to the solution, maintaining the temperature at 80 °C. Upon gel formation, the mixture underwent combustion, resulting in the formation of a black powder. The obtained powder was calcinated at 700 °C for 5 h.

Fabrication of Pt-perovskite-GCE Exosensor

To prepare a suspension of perovskite, 0.03 g of Pt-perovskite powder was ground and dispersed in 10 mL of distilled water. Then the obtained suspension was placed in an ultrasonic device for 2 h to disperse the nanocomposite well. Next, 2 mL of dispersed suspension and 8 mL of 0.1 M KCl were mixed and used for the electrodeposition of platinum perovskite through the chronoamperometric technique. In this regard, 10 mL of the obtained solution was transferred to the electrochemical cell. The deposition process was performed using the chronoamperometric (CHA) technique ($E = -2.4$ V, $t = 45$ s). Finally, the glassy carbon electrode modified with Pt-perovskite was applied for the next steps of analysis (Pt-per-GCE).

Surface functionalization

Biotinylated monoclonal CD63 antibody and streptavidin were incubated under optimal conditions according to previously published data [51]. In brief, to modify the biotinylated monoclonal CD63 antibody on the surface of Pt-per-GCE, the streptavidin (STRP) protein (1 μg mL^{-1}) was first incubated on the Pt-per-GCE at 4 °C for 90 min. STRP was used to increase the loading capacity of anti-CD63 immobilization. The STRP, due to its unique molecular structure, could provide more binding active sites, where the sensitivity of the developed Exosensor could increase four times [52]. Next, anti-CD63 (1 μg mL^{-1}) was introduced on the STRP-Pt-per-GCE for incubation at 4 °C for 90 min. Finally, 1 mg mL^{-1} MCH was applied to prevent nonspecific adsorption.

Cell culture and EV isolation

To calibrate the designed Exosensor, prostate cancer cell EVs were isolated, purified, and introduced to the Exosensor platform. Human prostate cancer DU145 cells were purchased from Iranian Cell Bank Pasture and cultured in DMEM/HG medium supplemented with 10% fetal bovine serum (FBS; Gibco) and 1% penicillin–streptomycin. Upon 70–80% confluence, cells were washed with pre-warmed PBS and incubated with EV-free FBS (Gibco). After 48-h incubation time, supernatants were collected and centrifuged at 400, 2000, and 10,000 g for 5, 10, and 20 min respectively to eliminate cells, debris, and apoptotic bodies. To get the EV pellet, samples were centrifuged at 100,000 g for 1 h. Finally, the morphology and zeta potential, and the number of EVs were approximately determined using SEM images and DLS analysis.

Result and discussion

Structure and morphology

Upon comparing the XRD pattern of the synthesized $La(Fe_{0.7}Mn_{0.3})_{0.98}Pt_{0.02}O_3$ catalyst (Figure S1) to the standard pattern of $LaFeO_3$ (01–075-0439), we observed that the synthesized nanocomposite exhibits an orthorhombic structure, similar to that of $LaFeO_3$. However, a slight shift towards higher angles (to the right) is observed in $La(Fe_{0.7}Mn_{0.3})_{0.98}Pt_{0.02}O_3$ structure. This shift may be attributed to the incorporation of Mn, which has a different ionic radius and consequently alters the unit cell size. Remarkably, the addition of Pt did not result in the emergence of distinct peaks, indicating that the noble metals do not significantly modify the perovskite host lattice [52–54]. The morphology of the prepared perovskite was examined using SEM and TEM (Fig. 1). SEM analysis revealed the agglomerated and non-uniform spherical nanoparticles. Furthermore, TEM images provided additional insights, showing that the nanoparticles have an average crystallite diameter of 40 nm. The surface elemental composition and oxidation states of $La(Fe_{0.7}Mn_{0.3})_{0.98}Pt_{0.02}O_3$ nanoparticles were analyzed using XPS (Fig. 2).

Figure 2A displays the XPS spectra of $La(Fe_{0.7}Mn_{0.3})_{0.98}Pt_{0.02}O_3$, indicating the presence of all

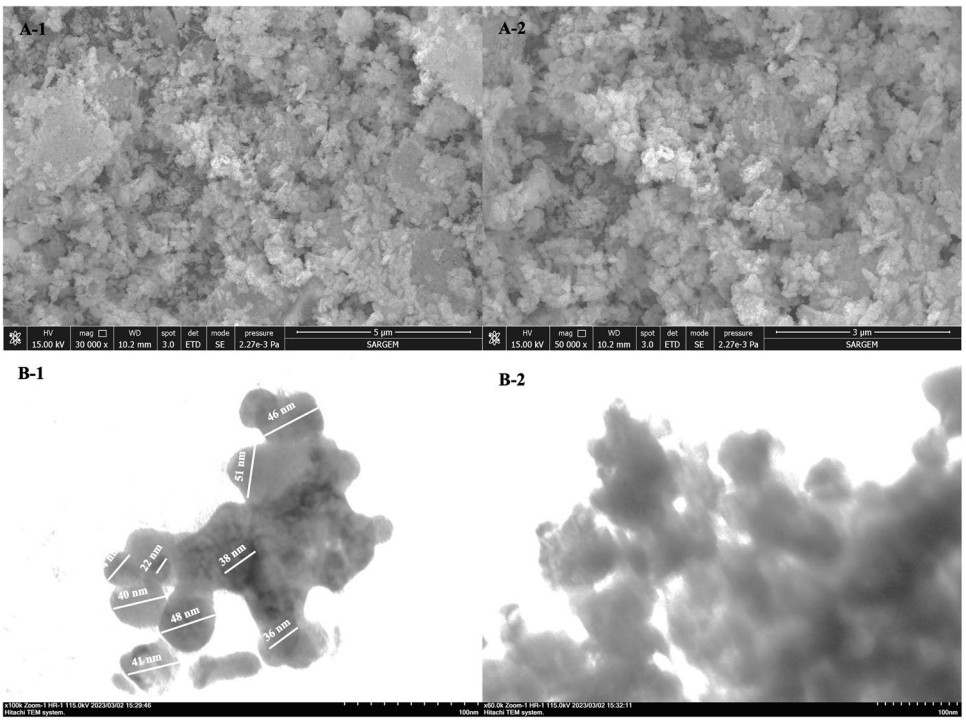

Fig. 1 SEM (a-1, a-2) and TEM (b-1, b-2) images of $La(Fe_{0.7}Mn_{0.3})_{0.98}Pt_{0.02}O_3$

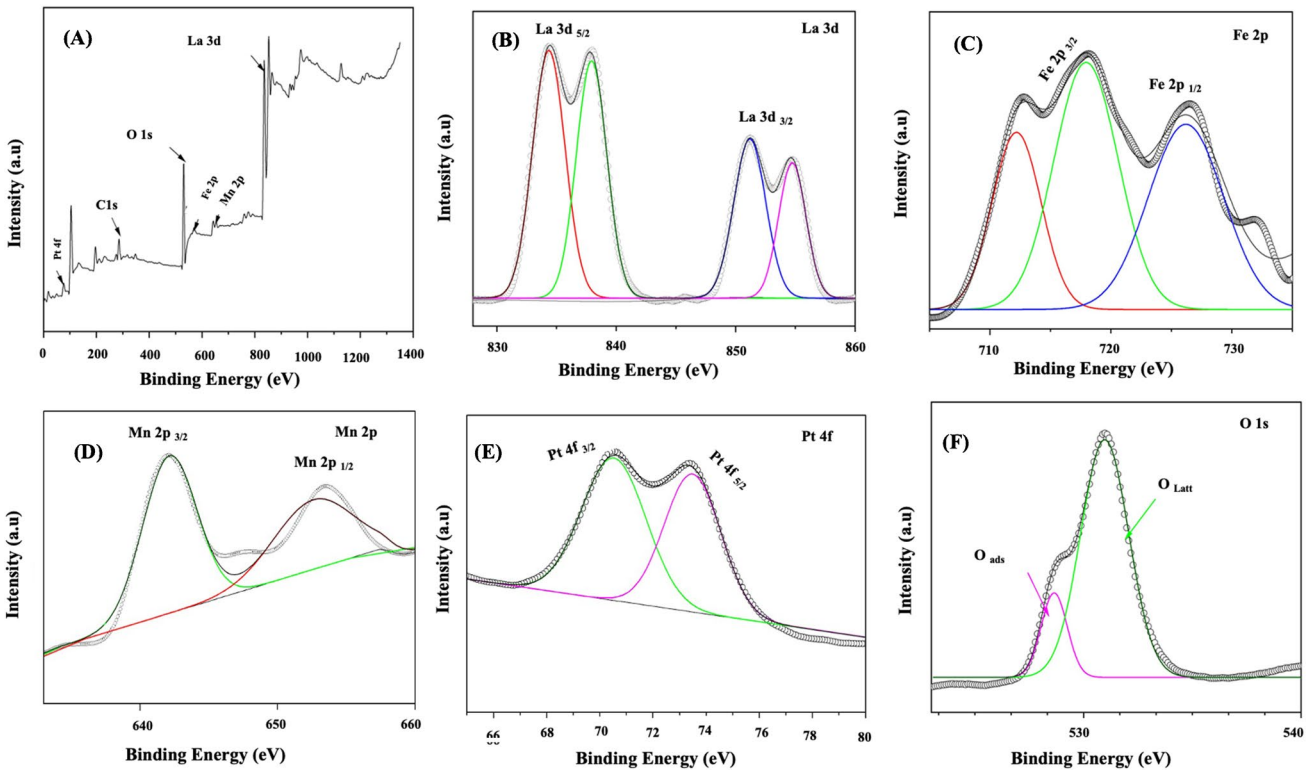

Fig. 2 XPS survey and elemental spectra of $La(Fe_{0.7}Mn_{0.3})_{0.98}Pt_{0.02}O_3$

elements within the perovskite structure. Figure 2B shows the XPS spectra of La 3d, with two doublet peaks corresponding to La $3d_{3/2}$ and $3d_{5/2}$. The peaks at 834.48 and 837.98 eV peaks correspond to La $3d_{5/2}$, while peaks around 851.28 and 854.68 eV are attributed to La $3d_{3/2}$. The presence of peaks at 854.78 and 834.48 eV confirms the La^{3+} oxidation state. The

other peaks may be due to charge transfer from neighboring La atoms to the vacant 4f subshell during ionization [54]. The Fe 2p spectra show two distinct peaks at binding energies of 712.413 eV and 726.18 eV, corresponding to the $2p_{3/2}$ and $2p_{1/2}$ levels, respectively. These peaks exhibited typical shake-up structures at 717.98 eV, indicative of ferric ions in oxide forms [55]. The Mn 2p XPS spectra (Fig. 2D) exhibit single peaks at 642.15 eV (Mn $2p_{3/2}$) and 652.66 eV (Mn $2p_{1/2}$), indicating the coexistence of Mn^{4+} and Mn^{3+} in the perovskite structure (Fig. 2C) [56]. In the Pt 4f spectra (Fig. 2E), the binding energies around 71.98 eV and 74 eV correspond to Pt $4f_{7/2}$ and Pt $4f_{5/2}$, indicating the presence of adsorbed oxygen (Pt_{Oads}) and oxidized Pt^{2+} [57]. The XPS spectra of O1s (Fig. 2F) display two asymmetric peaks at 528.88 eV and 531.18 eV, suggesting the presence of lattice oxygen and chemisorbed oxygen species. The binding energy of chemisorbed oxygen species (O^-/OH^-) is generally higher by 2.1–2.5 eV than that of lattice oxygen [58].

Optimization of electrodeposition potential

To improve the performance and sensitivity of the Exosensor and the effective surface of the electrode for loading the antibody, the perovskite density was optimized on the surface of the electrode using the chronoamperometric technique. For this purpose, the potential was optimized and the results were obtained using differential pulse voltammetry (DPV) in 5 mM $[Fe(CN)_6]^{3-/4}$/0.1 M KCl solution (pH 7.4) as an electrochemical redox system. In this regard, the range of potentials was selected from − 2.7 to − 2.2 V to reduce and deposit Pt-perovskite on the electrode surface [59]. Figure S2 shows the current generated from each of the potentials as well as the related histogram. Based on the results, the potential of − 2.4 V was chosen as the optimal potential for Pt-per electrodeposition on the electrode surface. Data confirmed that platinum, the active site of the composite, is lost when sweeping the potential towards positive potentials. These features cause a decrease in the current and consequently the performance in this analytical approach [60].

Optimization of electrodeposition time

For enhancing the efficacy of the designed Exosensor, the time of the electrodeposition of Pt-based perovskite nanocomposite was optimized using the chronoamperometric technique. In this regard, time intervals of 15 to 360 s were selected for optimization. Based on the obtained results, the maximum electric current was recorded in 45 s, which shows that there is enough time for nanocomposite deposition on the electrode surface. According to the data (Figure S3), with increasing time of chronoamperometry, the corresponding current gradually decreases because of excessive accumulation and saturation of the electrode surface with nanocomposite. Therefore, 45 s was selected as the optimal time for Pt-perovskite electrodeposition.

EV detection (electrode preparation steps)

The GCE was modified as mentioned. EVs at an appropriate concentration ($V = 15$ µL ~ 6000 EVs/µL) were incubated on STRP-Pt-per-GCE functionalized biotinylated monoclonal CD63 antibody at 4 °C for 60 min. Then the prepared Exosensor was placed in the electrochemical cell containing 5 mM $[Fe(CN)_6]^{3-/4-}$/0.1 M KCl solution (pH 7.4) to monitor the EV number (Fig. 3).

Electrochemical detection of EVs (calibration curve)

The developed Exosensor was applied for the quantification of different concentrations of EVs under the optimized conditions. For this purpose, semi-quantitative analysis was carried out on the EVs that were previously isolated with approximate numbers in certain volumes. Thus, different volumes were properly immobilized on the designed Exosensor and their related electrical signals were recorded by DPV technique in 5 mM $[Fe(CN)_6]^{3-/4-}$/0.1 M KCl solution (pH 7.4). As shown in Fig. 4, a linear relationship between the recorded electrical signal and the number of EVs with an equation of $Y = -1.7668x + 32.843$ ($R^2 = 0.9789$) was obtained, and the lower limit of quantitation (LLOQ) is 2000 EVs/µL. Based on the results of a calibration curve, the linear dynamic range (LDR) was reported to be 2000 to 14,000 EVs/µL. In Fig. 4, panels A and B show the related voltammograms and the average electric current versus the number of EVs.

Extracellular vesicle detection in clinical samples

Here, an Exosensor was designed to monitor prostate cancer EV PSA and data were compared to conventional ELISA assay (Fig. 5). ELISA indicated that prostate cancer marker PSA levels were high in prostate cancer patients compared to the healthy control individual. The difference in PSA levels in cancer patients can correlate with the tumor size and progression of anaplastic changes [9]. Our laboratory data indicated that systemic levels of PSA increase in patients with the relevant prostate cancer manifestation. To examine whether prostate cancer EVs harbor specific PSA and investigate the close relationship between the blood content and exosomal levels, the protein contents of PSA were measured using the Exosensor. Based on the data, the electrical current of PSA-modified electrodes was recorded as the same as the calibration curve. We noted statistically significant differences regarding the electrical current between EV PSA in prostate cancer patients and healthy control samples ($p < 0.0001$; Fig. 5). It is postulated that attachment of

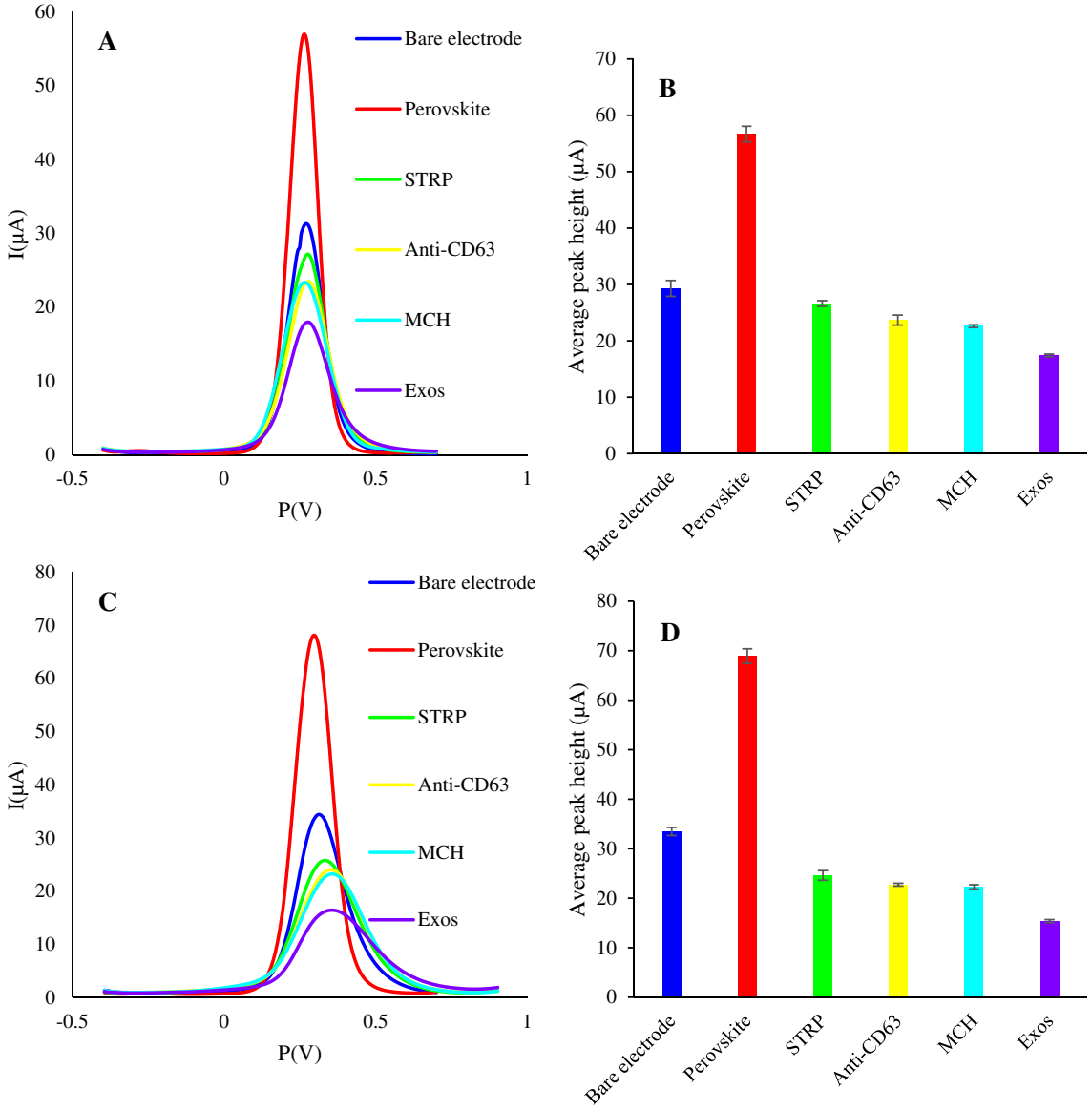

Fig. 3 Electrode preparation steps: DPV signals (**A**) and its related histogram (**B**). SWV signals (**C**) and related histogram (**D**). All experiments were performed in 5 mM $[Fe(CN)6]^{3-/4-}$/0.1 M KCl (pH 7.4) solution

anti-PSA antibody to EVs yielded lower electrical current (μA) values in prostate cancer patients. Of note, the reduction of μA was prominent in samples with higher levels of PSA measured by ELISA. To be specific, in prostate cancer patient 3, the levels of systemic PSA were 35.9 U/mL with 3.9 μA indicated by Exosensor. Data indicated that by increasing the levels of Exosomal PSA, the intensity of the electrical current is reduced in which EVs of prostate cancer patient 3 had the lowest electrical current (μA) value compared to EVs of prostate cancer patients 1 and 2. These data show that the levels of exosomal PSA are increased with the progression of anaplastic changes in prostate cancer. Like blood samples, EVs can appropriately reflect real-time changes in prostate cancer patients. The main features of the most recent electrochemical biosensors, which diagnose various illnesses by analyzing linked EVs, are outlined in Table 1.

By generating geno/apta/immuno/sensors for evaluation of EVs, various nanomaterials were used to study different cancers. The performance of noted electrochemical biosensors is comparable in a number of ways: (I) the nanomaterial used in electrode modification should be biocompatible and cost-effective [44, 45, 64, 65]; (II) analytical performances such as linear dynamic range, sensitivity, and selectivity should have the highest levels; and (III) the working electrodes and techniques used must be suitable for theragnostic purposes. Table 1 shows that

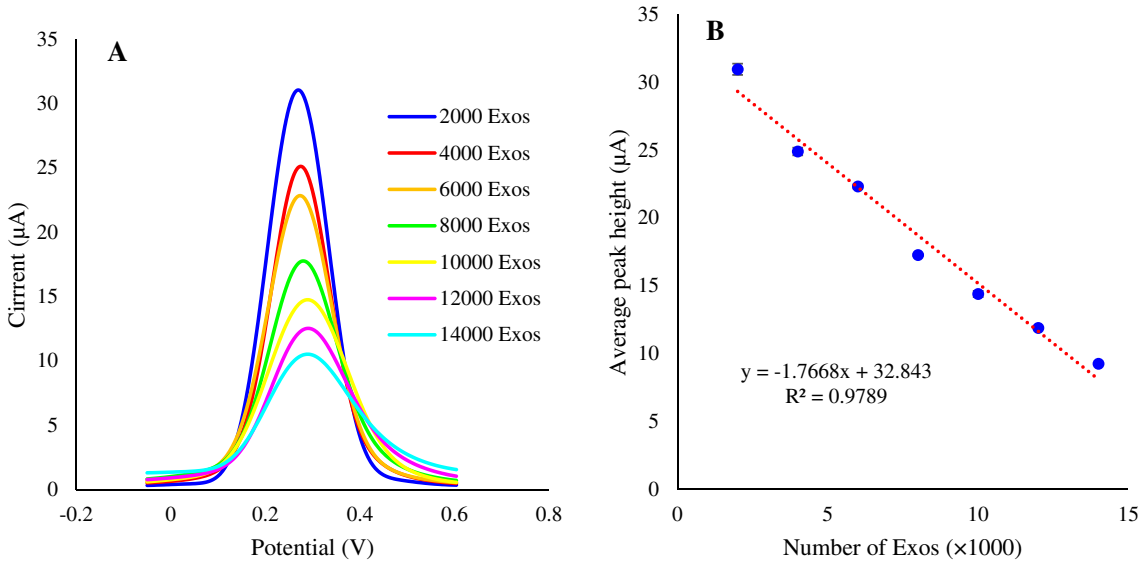

Fig. 4 **A** DPV signal readouts and (**B**) calibration curve for different numbers of the EVs. Error bars indicate the standard deviation of ten independent experiments

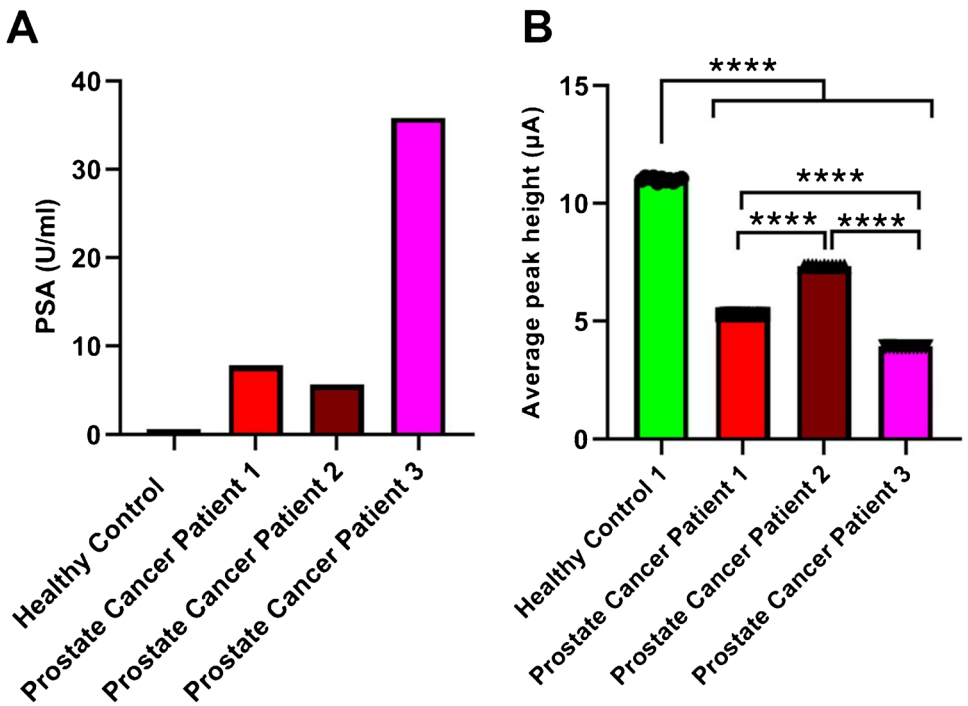

Fig. 5 Measuring the levels of PSA using ELISA (**A**) and Exosensor (**B**). ELISA indicates the increase of PSA levels in prostate cancer patients compared to the healthy control. Designed Exosensor is eligible to detect different contents of exosomal PSA in both control and cancer patient samples. Data indicate the fluctuation in terms of PSA in patients with different prostate cancer stages. By the progression of prostate cancer, the recorded electrical signals are correspondingly reduced, showing the sensitivity of designed Exosensor in the validation of PSA in biological samples. One-way ANOVA and Tukey post hoc analysis. ****$p < 0.0001$. Each sample was read in 10 technical replicates

our developed biosensor is the most sensitive approach among previously reported works. Our research work has desirable lower limit of quantification (LLOQ) among others, which appears to be due to the presence of perovskite nanostructure and platinum nanoparticles. This nanocomposite as modifier increases the effective surface area and catalyzes the electrochemical reaction on the electrode, which in consequently enhances the sensitivity in detecting target EVs. The results of our work show that the modified electrodes have desirable stability because the modifiers are properly attached on the electrode surface. The techniques that are most common are DPV and SWV, which are used in the fabrication of electrochemical biosensors due to their low detection limits and high sensitivities.

Table 1 Comparison of different electrochemical biosensors for evaluation of EVs

Nanomaterials	Working electrode	Detection technique	LOD/LLOQ	Linear range	Source	Ref
Magnetic beads	Gold electrode	Chronoamperometry	3×10^4 EVs μL^{-1}	-	Ovarian cancer	[61]
Magnetic particles	graphite and epoxy resin	Amperometry	10^5 EVs μL^{-1}	-	Breast cancer	[62]
UiO-66 MOF	Gold electrode	SWV	7.83×10^3 EVs μL^{-1}	9.5×10^3 to 1.9×10^7 EVs μL^{-1}	Brain cancer	[24]
-	Screen-printed carbon electrode	DPV	4.7×10^5 EVs μL^{-1}	2.35×10^6 to 1.5×10^8 EVs μL^{-1}	Breast cancer	[63]
Pt-provskite	Glassy carbon electrode	DPV	2×10^3 EVs μL^{-1}	2×10^3 to 14×10^3 EVs μL^{-1}	Prostate cancer	This work

Real sample collection

EVs were isolated from blood sample remnants of prostate cancer patients who referred to Shahid Ghazi Hospital affiliated to Tabriz University of Medical Sciences. EVs were isolated using similar protocols described for the isolation of EVs from cell culture samples. All phases of this study were approved by local ethics committee of Tabriz University of Medical Sciences and steps were in accordance with previously published guidelines of the Declaration of Helsinki.

Statistical analysis

In this study, data are expressed as mean ± SD. To compare statistical differences between the groups, one-way ANOVA with post hoc analysis was used. $p < 0.05$ was considered statistically significant.

Conclusion

In this research, an electrochemical Exosensor was successfully designed for prostate cancer derived-extracellular vesicles analysis. For this purpose, platinum-based perovskite nanostructures were synthesized as modifying nanomaterials. The advantages of these nanostructures can be mentioned as high conductivity and surface area, biocompatibility, and cost-effectiveness. The existence of the noble platinum metal as an active site provides the possibility of better binding of streptavidin and then antibody on the surface of the electrode. Based on this, simultaneously the stability and the sensitivity of the prepared Exosensor improved. The detection method is based on the specific binding of biotinylated monoclonal anti-CD63 and anti-PSA to EVs through the sandwiching method to determine prostate cancer EVs. Among the applications of this designed Exosensor, we can point out the differentiation between normal and tumorous EVs, which leads to the evaluation of the early stages of PSA. Also, this developed method can be used as a POC test in clinical laboratories.

Supplementary Information The online version contains supplementary material available at https://doi.org/10.1007/s00604-024-06655-z.

Acknowledgements The authors gratefully acknowledge the Tabriz University for support.

Author contribution "Ehsan Dezhakam was contributed in all experimental analysis and preparing of first draft. Elham Mahmoudi, Aligholi Niaei, Nagihan Delibas and Ali Coruh helped in nanomaterial synthesis, charachterization and related interpretations. Abdolhossein Naseri supervised the study and assisted data interpretations and editing. Reza Rahbarghazi supervised the study and helped editing. Ibrahim Isildak assisted in validation of data and editing. Balal Khalilzadeh was supervised the study and participated in idea, development of the method, validation of data and editing. All authors reviewed the manuscript."

Funding This project was financially supported by Stem Cell Research Center, Tabriz University of Medical Sciences, Tabriz, Iran (Grant number: 73720).

Data availability No datasets were generated or analysed during the current study.

Declarations

Ethics approval and consent to participate All patients were asked to complete the informed consent before the application of sera. All procedures of this study were approved by the Local Ethics Committee of Tabriz University of Medical Sciences (IR.TBZMED.REC.1403.409). All procedures were done under the declaration of Helsinki.

Competing interests The authors declare no competing interests.

References

1. Mardi N, Haiaty S, Rahbarghazi R, Mobarak H, Milani M, Zarebkohan A, Nouri M (2023) Exosomal transmission of viruses, a two-edged biological sword. Cell Communication and Signaling 21(1):1–29
2. Dezhakam E, Khalilzadeh B, Naseri A, Rahbarghazi R, Mahmoudi E, Niaei A, Mahdipour M, Mardi N, Isildak I (2024) Direct profiling of breast cancer-derived extracellular vesicles using Pd-perovskite electrochemical biosensing platform. Cancer Nanotechnol 15(1):1–16
3. Heidarzadeh M, Zarebkohan A, Rahbarghazi R, Sokullu E (2023) Protein corona and exosomes: new challenges and prospects. Cell Commun Signaling 21(1):1–15

4. Nasrollahpour H, Khalilzadeh B, Naseri A, Yousefi H, Erk N, Rahbarghazi R (2022) Electrochemical biosensors for stem cell analysis; applications in diagnostics, differentiation and follow-up. TrAC, Trends Anal Chem 156:116696
5. Fang X, Duan Y, Adkins GB, Pan S, Wang H, Liu Y, Zhong W (2018) Highly efficient exosome isolation and protein analysis by an integrated nanomaterial-based platform. Anal Chem 90(4):2787–2795
6. Dezhakam E, Khalilzadeh B, Mahdipour M, Isildak I, Yousefi H, Ahmadi M, Naseri A, Rahbarghazi R (2022) Electrochemical biosensors in exosome analysis; a short journey to the present and future trends in early-stage evaluation of cancers. Biosens Bioelectron 222:114980. https://doi.org/10.1016/j.bios.2022.114980
7. Nasrollahpour H, Mirzaie A, Sharifi M, Rezabakhsh A, Khalilzadeh B, Rahbarghazi R, Yousefi H, Klionsky DJ (2024) Biosensors; a novel concept in real-time detection of autophagy. Biosensors Bioelectronics 254:116204
8. Liu C, Zhao J, Tian F, Cai L, Zhang W, Feng Q, Chang J, Wan F, Yang Y, Dai B (2019) Low-cost thermophoretic profiling of extracellular-vesicle surface proteins for the early detection and classification of cancers. Nature Biomed Eng 3(3):183–193
9. Nasrollahpour H, Khalilzadeh B, Naseri A, Mamaghani S, Isildak I, Rashidi M-R (2023) Chitosan/luminol/AgNPs nanocomposite for electrochemiluminescent determination of prostate-specific antigen. Microchim Acta 190(3):90
10. Kordelas L, Rebmann V, Ludwig A, Radtke S, Ruesing J, Doeppner T, Epple M, Horn P, Beelen D, Giebel B (2014) MSC-derived exosomes: a novel tool to treat therapy-refractory graft-versus-host disease. Leukemia 28(4):970–973
11. Van Der Pol E, Hoekstra A, Sturk A, Otto C, Van Leeuwen T, Nieuwland R (2010) Optical and non-optical methods for detection and characterization of microparticles and exosomes. J Thromb Haemost 8(12):2596–2607
12. Nolte-t Hoen EN, van der Vlist EJ, Aalberts M, Mertens HC, Bosch BJ, Bartelink W, Mastrobattista E, van Gaal EV, Stoorvogel W, Arkesteijn GJ (2012) Quantitative and qualitative flow cytometric analysis of nanosized cell-derived membrane vesicles. Nanomed: Nanotechnol Biol Med 8(5):712–720
13. Jørgensen MM, Bæk R, Varming K (2015) Potentials and capabilities of the Extracellular Vesicle (EV) Array. J Extracellular Vesicles 4(1):26048
14. Yu Y, Li Y-T, Jin D, Yang F, Wu D, Xiao M-M, Zhang H, Zhang Z-Y, Zhang G-J (2019) Electrical and label-free quantification of exosomes with a reduced graphene oxide field effect transistor biosensor. Anal Chem 91(16):10679–10686
15. Fu Y, Ma Q (2020) Recent developments in electrochemiluminescence nanosensors for cancer diagnosis applications. Nanoscale 12(26):13879–13898
16. Cheng N, Du D, Wang X, Liu D, Xu W, Luo Y, Lin Y (2019) Recent advances in biosensors for detecting cancer-derived exosomes. Trends Biotechnol 37(11):1236–1254
17. Zhou Y, Xu H, Wang H, Ye B-C (2020) Detection of breast cancer-derived exosomes using the horseradish peroxidase-mimicking DNAzyme as an aptasensor. Analyst 145(1):107–114
18. Fan Y, Duan X, Zhao M, Wei X, Wu J, Chen W, Liu P, Cheng W, Cheng Q, Ding S (2020) High-sensitive and multiplex biosensing assay of NSCLC-derived exosomes via different recognition sites based on SPRi array. Biosens Bioelectron 154:112066
19. Ning C-F, Wang L, Tian Y-F, Yin B-C, Ye B-C (2020) Multiple and sensitive SERS detection of cancer-related exosomes based on gold–silver bimetallic nanotrepangs. Analyst 145(7):2795–2804
20. Huang R, He L, Li S, Liu H, Jin L, Chen Z, Zhao Y, Li Z, Deng Y, He N (2020) A simple fluorescence aptasensor for gastric cancer exosome detection based on branched rolling circle amplification. Nanoscale 12(4):2445–2451
21. Fang D, Zhao D, Zhang S, Huang Y, Dai H, Lin Y (2020) Black phosphorus quantum dots functionalized MXenes as the enhanced dual-mode probe for exosomes sensing. Sens Actuators, B Chem 305:127544
22. Wu D, Yu Y, Jin D, Xiao M-M, Zhang Z-Y, Zhang G-J (2020) Dual-aptamer modified graphene field-effect transistor nanosensor for label-free and specific detection of hepatocellular carcinoma-derived microvesicles. Anal Chem 92(5):4006–4015
23. Baek E, Rim T, Schütt J, Baek C-k, Kim K, Baraban L, Cuniberti G (2017) Negative photoconductance in heavily doped Si nanowire field-effect transistors. Nano Lett 17(11):6727–6734
24. Sun Z, Wang L, Wu S, Pan Y, Dong Y, Zhu S, Yang J, Yin Y, Li G (2020) An electrochemical biosensor designed by using Zr-based metal–organic frameworks for the detection of glioblastoma-derived exosomes with practical application. Anal Chem 92(5):3819–3826
25. Zhang Y, Wang X (2020) Targeting the Wnt/β-catenin signaling pathway in cancer. J Hematol Oncol 13(1):165. https://doi.org/10.1186/s13045-020-00990-3
26. Sohrabi H, Dezhakam E, Khataee A, Nozohouri E, Majidi MR, Mohseni N, Trofimov E, Yoon Y (2022) Recent trends in layered double hydroxides based electrochemical and optical (bio) sensors for screening of emerging pharmaceutical compounds. Environ Res 211:113068
27. Sohrabi H, Dezhakam E, Nozohouri E, Majidi MR, Orooji Y, Yoon Y, Khataee A (2022) Advances in layered double hydroxide based labels for signal amplification in ultrasensitive electrochemical and optical affinity biosensors of glucose. Chemosphere 309:136633
28. Mirzaie A, Nasrollahpour H, Khalilzadeh B, Jamali AA, Spiteri RJ, Yousefi H, Isildak I, Rahbarghazi R (2023) Cerebrospinal fluid: a specific biofluid for the biosensing of Alzheimer's diseases biomarkers. TrAC Trends Anal Chem 166:117174
29. Nasrollahpour H, Khalilzadeh B (2023) Naked eye biosensors for pathogen monitoring. TrAC Trends Anal Chem 166:117499
30. Maduraiveeran G, Sasidharan M, Ganesan V (2018) Electrochemical sensor and biosensor platforms based on advanced nanomaterials for biological and biomedical applications. Biosens Bioelectron 103:113–129
31. Dezhakam E, Tavakkol M, Kafili T, Nozohouri E, Naseri A, Khalilzadeh B, Rahbarghazi R (2023) Electrochemical and optical (bio) sensors for analysis of antibiotic residuals. Food Chem 439(1):138145. https://doi.org/10.1016/j.foodchem.2023.138145
32. Wu Q, Miao W-s, Zhang Y-d, Gao H-j, Hui D (2020) Mechanical properties of nanomaterials: a review. Nanotechnol Rev 9(1):259–273
33. Wang L, Li J, Feng M, Min L, Yang J, Yu S, Zhang Y, Hu X, Yang Z (2017) Perovskite-type calcium titanate nanoparticles as novel matrix for designing sensitive electrochemical biosensing. Biosens Bioelectron 96:220–226
34. Yashas SR, Sandeep S, Shivakumar BP, Swamy NK (2019) A matrix of perovskite micro-seeds and polypyrrole nanotubes tethered laccase/graphite biosensor for sensitive quantification of 2, 4-dichlorophenol in wastewater. Anal Methods 11(35):4511–4519
35. Cai B, Zhao M, Wang Y, Zhou Y, Cai H, Ye Z, Huang J (2014) A perovskite-type KNbO3 nanoneedles based biosensor for direct electrochemistry of hydrogen peroxide. Ceram Int 40(6):8111–8116
36. Yokokawa H, Sakai N, Kawada T, Dokiya M (1992) Thermodynamic stabilities of perovskite oxides for electrodes and other electrochemical materials. Solid State Ionics 52(1–3):43–56

37. Tsvetkov N, Lu Q, Sun L, Crumlin EJ, Yildiz B (2016) Improved chemical and electrochemical stability of perovskite oxides with less reducible cations at the surface. Nat Mater 15(9):1010–1016
38. Islam QA, Paydar S, Akbar N, Zhu B, Wu Y (2021) Nanoparticle exsolution in perovskite oxide and its sustainable electrochemical energy systems. J Power Sources 492:229626
39. He J, Xu X, Li M, Zhou S, Zhou W (2023) Recent advances in perovskite oxides for non-enzymatic electrochemical sensors: a review. Anal Chim Acta 1251:341007
40. Nezhad PDK, Bekheet MF, Bonmassar N, Gili A, Kamutzki F, Gurlo A, Doran A, Schwarz S, Bernardi J, Praetz S (2022) Elucidating the role of earth alkaline doping in perovskite-based methane dry reforming catalysts. Catal Sci Technol 12(4):1229–1244
41. Ahangari M, Mostafaei J, Sayyah A, Mahmoudi E, Asghari E, Coruh A, Delibas N, Niaei A (2023) Investigation of structural and electrochemical properties of SrFexCo1-xO3-δ perovskite oxides as a supercapacitor electrode material. J Energy Storage 63:107034
42. Gargari MR, Mahmoudi E, Majidi MM, Sohrabi H, Majidi MR, Niaei A (2023) Mesoporous perovskite-type La0. 8Sr0. 2Cu0. 7Mn0. 3O3/SiO2 nanocomposite-decorated-graphene-oxide nanosheets: green synthesis and application in the sensitive determination of Morin in kiwi fruit samples. Synthetic Metals 293:117257
43. Yu J, Wu X, Guan D, Hu Z, Weng S-C, Sun H, Song Y, Ran R, Zhou W, Ni M (2020) Monoclinic SrIrO3: an easily synthesized conductive perovskite oxide with outstanding performance for overall water splitting in alkaline solution. Chem Mater 32(11):4509–4517
44. Mahmoudi E, Asghari E, Delibaş N, Niaei A (2023) Application of response surface methodology for optimization of the test condition of oxygen evolution reaction over La0. 8Ba0. 2CoO3 perovskite-active carbon composite. Scientific Reports 13(1):22878
45. Mahmoudi E, Mostafaei J, Griesser C, Bekheet MF, Delibas N, Penner S, Asghari E, Coruh A, Niaei A (2023) LaCoO3-BaCoO3 porous composites as efficient electrocatalyst for oxygen evolution reaction. Chem Eng J 473:144829
46. Choi M, Ibrahim IA, Kim K, Koo JY, Kim SJ, Son J-W, Han JW, Lee W (2020) Engineering of charged defects at perovskite oxide surfaces for exceptionally stable solid oxide fuel cell electrodes. ACS Appl Mater Interfaces 12(19):21494–21504
47. Dai Y, Yu J, Cheng C, Tan P, Ni M (2020) Mini-review of perovskite oxides as oxygen electrocatalysts for rechargeable zinc–air batteries. Chem Eng J 397:125516
48. Nan H-s, Hu X-y, Tian H-w (2019) Recent advances in perovskite oxides for anion-intercalation supercapacitor: a review. Mater Sci Semicond Process 94:35–50
49. Yan Y, Wang T, Li X, Pang H, Xue H (2017) Noble metal-based materials in high-performance supercapacitors. Inorganic Chem Front 4(1):33–51
50. Hosseini SA, Mehri B, Niaei A, Izadkhah B, Alvarez-Galvan C, Fierro JGL (2018) Selective catalytic reduction of NO x by CO over LaMnO 3 nano perovskites prepared by microwave and ultrasound assisted sol–gel method. J Sol-Gel Sci Technol 85:647–656
51. Sadi S, Khalilzadeh B, Mahdipour M, Sokouti Nasimi F, Isildak I, Davaran S, Rashidi M-R, Bani F (2023) Early stage evaluation of cancer stem cells using platinum nanoparticles/CD133+ enhanced nanobiocomposite. Cancer Nanotechnology 14(1):55
52. Tarjomannejad A, Farzi A, Gómez MJI, Niaei A, Salari D, Albaladejo-Fuentes V (2016) Catalytic reduction of NO by CO over LaMn 1–x Fe x O 3 and La 0.8 A 0.2 Mn 0.3 Fe 0.7 O 3 (A= Sr, Cs, Ba, Ce) perovskite catalysts. Catal Lett 146:2330–2340
53. Sacco O, Stoller M, Vaiano V, Ciambelli P, Chianese A, Sannino D (2012) Photocatalytic degradation of organic dyes under visible light on N-doped TiO 2 photocatalysts. Int J Photoenergy 1:626759. https://doi.org/10.1155/2012/626759
54. Jørgensen C, Berthou H (1972) Split photo-electron signals from the unique closed-shell cation lanthanum (III). Chem Phys Lett 13(3):186–189
55. Thirumalairajan S, Girija K, Mastelaro VR, Ganesh V, Ponpandian N (2014) Detection of the neurotransmitter dopamine by a glassy carbon electrode modified with self-assembled perovskite LaFeO 3 microspheres made up of nanospheres. RSC Adv 4(49):25957–25962
56. Mao M, Xu J, Li Y, Liu Z (2020) Hydrogen evolution from photocatalytic water splitting by LaMnO 3 modified with amorphous CoS x. J Mater Sci 55:3521–3537
57. Ohtani B, Iwai K, Nishimoto S-i, Sato S (1997) Role of platinum deposits on titanium (IV) oxide particles: structural and kinetic analyses of photocatalytic reaction in aqueous alcohol and amino acid solutions. J Phys Chem B 101(17):3349–3359
58. Rida K, Benabbas A, Bouremmad F, Pena M, Sastre E, Martínez-Arias A (2007) Effect of calcination temperature on the structural characteristics and catalytic activity for propene combustion of sol–gel derived lanthanum chromite perovskite. Appl Catal A 327(2):173–179
59. Nasrollahpour H, Mahdipour M, Isildak I, Rashidi M-R, Naseri A, Khalilzadeh B (2021) A highly sensitive electrochemiluminescence cytosensor for detection of SKBR-3 cells as metastatic breast cancer cell line: a constructive phase in early and precise diagnosis. Biosens Bioelectron 178:113023
60. Sadi S, Khalilzadeh B, Mahdipour M, Sokouti Nasimi F, Isildak I, Davaran S, Rashidi M-R, Bani F (2023) Early stage evaluation of cancer stem cells using platinum nanoparticles/CD133+ enhanced nanobiocomposite. Cancer Nanotechnol 14(1):1–15
61. Jeong S, Park J, Pathania D, Castro CM, Weissleder R, Lee H (2016) Integrated magneto–electrochemical sensor for exosome analysis. ACS Nano 10(2):1802–1809
62. Moura SL, Martín CG, Martí M, Pividori MI (2020) Electrochemical immunosensing of nanovesicles as biomarkers for breast cancer. Biosens Bioelectron 150:111882
63. Yadav S, Boriachek K, Islam MN, Lobb R, Möller A, Hill MM, Hossain MSA, Nguyen NT, Shiddiky MJ (2017) An electrochemical method for the detection of disease-specific exosomes. ChemElectroChem 4(4):967–971
64. Shariatinia Z, Karimzadeh Z (2024) Perovskite oxides as efficient bioactive inorganic materials in tissue engineering: a review. Mater Today Chem 35:101846
65. Gong J, Xu T (2020) Perovskite materials in biomedical applications. Revolution of perovskite: synthesis, properties and applications. Revolution of Perovskite. 95–116